6-10-2012

Detecting gravitational wave memory with pulsar timing

J. M. Cordes

F. A. Jenet

Recommended Citation

J. M. Cordes, et. al., (2012) Detecting gravitational wave memory with pulsar timing.Astrophysical Journal752:1. DOI: http://doi.org/10.1088/0004-637X/752/1/54

The Astrophysical Journal, 752:54 (8pp), 2012 June 10 doi:10.1088/0004-637X/752/1/54

DETECTING GRAVITATIONAL WAVE MEMORY WITH PULSAR TIMING

J. M. Cordes[1] and F. A. Jenet[2]
[1] Astronomy Department, Cornell University, Ithaca, NY 14853, USA; cordes@astro.cornell.edu
[2] Center for Gravitational Wave Astronomy, University of Texas, Brownsville, TX 78520, USA; merlyn@phys.utb.edu
Received 2012 February 4; accepted 2012 April 10; published 2012 May 24

ABSTRACT

We compare the detectability of gravitational bursts passing through the solar system with those passing near each millisecond pulsar in an *N*-pulsar timing array. The sensitivity to Earth-passing bursts can exploit the correlation expected in pulse arrival times while pulsar-passing bursts, though uncorrelated between objects, provide an *N*-fold increase in overall time baseline that can compensate for the lower sensitivity. Bursts with memory from mergers of supermassive black holes produce step functions in apparent spin frequency that are the easiest to detect in pulsar timing. We show that the burst rate and amplitude distribution, while strongly dependent on inadequately known cosmological evolution, may favor detection in the pulsar terms rather than the Earth timing perturbations. Any contamination of timing data by red spin noise makes burst detection more difficult because both signals grow with the length of the time data span T. Furthermore, the different bursts that could appear in one or more data sets of length $T \approx 10$ yr also affect the detectability of the gravitational wave stochastic background that, like spin noise, has a red power spectrum. A burst with memory is a worthwhile target in the timing of multiple pulsars in a globular cluster because it should produce a correlated signal with a time delay of less than about 10 years in some cases.

Key words: gravitational waves – methods: statistical – pulsars: general

Online-only material: color figure

1. INTRODUCTION

Large efforts are underway for using ensembles of millisecond pulsars (MSPs) in pulsar timing arrays (PTAs) to detect gravitational waves with periods $\gtrsim$1 yr. Detection methods have targeted isotropic stochastic backgrounds, oscillatory or chirped signals from individual sources, and gravitational wave (GW) bursts. GW bursts are expected from high-mass systems in the universe that undergo catastrophic transformation, such as supernovae, inspirals and coalescence of compact stars, and mergers of supermassive black holes (SMBHs). Of these, only SMBHs are realistic targets for PTAs. The prospects for using pulsar timing techniques to detect burst sources have been discussed by Finn & Lommen (2010). Recently, there has been particular interest in detecting the "memory" term in bursts associated with SMBH binary inspirals (Seto 2009; van Haasteren & Levin 2010; Pshirkov et al. 2010). At relatively early stages, the chirped waveforms from inspiraling sources are potentially detectable in the bandpasses of interferometric detectors such as LIGO, LISA, and others (Pitkin et al. 2011). Our interest is in the final stage where the GW signal is the strongest and a long-term change in dimensionless strain can occur that is most easily detectable with pulsar timing. The advantage of pulsar timing is that the memory effect appears as a sudden change in pulse frequency that produces a secularly increasing amplitude in a sequence of arrival times.

Pulsar-timing-based GW detection techniques use both the Earth and the pulsar as "test masses." GWs influence the space-time around both masses thus influencing the time-of-flight of a pulse traveling between the pulsar and the Earth. When a GW arrives at the Earth, its effect is detectable immediately. Since pulsar signals must travel through the same space-time near the Earth, the Earth-term timing fluctuations are correlated for different pulsars while the pulsar terms are uncorrelated. GWs that arrive at the pulsar can take up to the light travel time between the Earth and the pulsar before their effects are manifested. In this work, we show how this delay can greatly increase our chances of detecting GW bursts with memory (BWM) from SMBH mergers as well as other possible burst sources.

Recent work on detecting BWMs using pulsars (Seto 2009; van Haasteren & Levin 2010; Pshirkov et al. 2010) has concentrated on the correlated Earth term of the timing perturbation because detection can be both enhanced and corroborated by exploiting the correlated signal. Similarly, a lack of correlation can be used to identify pulsar specific phenomena such as spin noise or interstellar propagation effects.

In this paper, we investigate the merits of the pulsar term in a search for GW bursts. The basic point is easily demonstrated. Consider the simple case where the average number of bursts per unit time is η. Assuming, for sake of argument, that we can detect every burst that occurs and distinguish it from other timing irregularities, the number of bursts detected in the Earth term for a given pulsar is ηT, where T is the total data span. Now consider a pulsar term. It contains information about the GW signals at a pulsar at a time D/c earlier than the Earth term but which are measured at a time $(D/c)(1 - \cos\theta)$ *later* than the Earth term, where D is the pulsar distance, c is the speed of light, and θ is the angular separation of the pulsar and the burst source. Since the delay D/c is typically hundreds to thousands of years, the pulsar term probes an epoch distinct from the Earth term. The expected number of bursts detected in both terms is $\sim 2\eta T$, the factor of two accounting for the fact that the Earth and pulsar terms probe non-overlapping time intervals. In general, if one observes N_p pulsars, the average number of detected bursts will be as high as $(N_p + 1)\eta T$. In practice, we expect the event rate of detectable events to be small, $\eta \lesssim 1/N_p T$, so our analysis includes consideration of the likelihood function for the burst rate that makes use of detections and non-detections in the Earth terms as well as the pulsar terms.

A burst source can be localized on the sky by using the relative amplitudes of the Earth terms in the timing residuals for different pulsars in a PTA (Finn & Lommen 2010). In principle, it is also possible to constrain the direction if the *same* burst were seen

in two or more pulsar terms. Conversely, some directions can be ruled out in the likely case that a burst is seen in only one of the pulsar terms.[3] It is unlikely that any given burst will be seen in more than one pulsar term for current data sets of length 5–10 years, at least for MSPs in the Galactic disk. In a population of N_p pulsars distributed uniformly out to a distance $D_{\rm max}$, the probability of a burst appearing in two of the pulsar terms $\sim cT/D_{\rm max} \approx 0.3\%$ for $T = 10$ yr and $D_{\rm max} = 1$ kpc. We have verified the probability of a two-fold detection by Monte Carlo simulations. For pulsar samples $N_p \lesssim 300$, a specific burst will be seen at most only singly in the Earth term or in one of the pulsar terms. Clearly, an MSP sample more concentrated toward the Sun has a greater chance of providing a joint detection. However, the probability of approximate simultaneity of two pulsar-term events is multiplied by the probability $\approx \eta T$ (for $\eta T \ll 1$) of having a burst occur at the right time for it to be seen in any of the terms. It is likely that the aggregate burst rate from all sources is small, so we do not pursue further the possibilities for source localization using bursts.

The issues of signal detection complicate matters because the correlated Earth terms provide greater sensitivity to GWs than a pulsar term. The added benefit of the pulsar terms depends on the distribution of burst strengths and on the details of the detection algorithm. The sensitivity of the Earth term to a BWM scales as $\sqrt{N_p}$, since the time series can be summed coherently, thus increasing the distance and total volume that are sampled. However, the pulsar terms extend the overall time baseline to N_pT due to the different directions and large distances to the pulsars. Whether the temporal or the volume factor dominates depends on the source population. The advantage of the pulsar term becomes clear when considering very large, but rare bursts that are well above the detection threshold even in a single pulsar data set. In this case, the $\sqrt{N_p}$ improvement from the Earth terms does not aid detection, whereas the longer temporal baseline may be key to detecting a burst.

A disadvantage of using the pulsar term is the lack of correlation between time series from different pulsars, which makes it harder to assess the burst interpretation against other possibilities and does not allow the burst direction to be localized. van Haasteren & Levin (2010) argue that events occurring only in the pulsar term of a particular pulsar cannot be distinguished from an intrinsic spin glitch, i.e., a discontinuity in the spin rate and its time derivative. Such glitches are not uncommon in young pulsars with large spin-down rates, but only one has been seen in an MSP (Cognard & Backer 2004). The specific object (B1821−24) has one of the largest period derivatives among MSPs so the glitch and related timing noise are not surprising. Glitch signatures usually show a decay or recovery after the discontinuity in spin frequency and are accompanied by discontinuities in spin-down rate. The BWM signature is a discontinuity only in spin frequency without any decay and thus in principle can be distinguished from glitches. In practice, distinguishing a glitch from a BWM will require frequent arrival-time sampling and sufficient signal-to-noise ratio (S/N) to rule out any decay or accompanying jump in spin-frequency derivative.

In Section 2, we review the GW burst phenomenon and the expected signature in pulsar timing data. In Section 3, a detection technique is described that allows us to identify burst events in individual pulsar data streams in the presence of additive white and red noise. We also present an example likelihood analysis that shows how event rates can be constrained in several hypothetical cases involving non-detections or detections in the Earth and pulsar terms. In Section 4 we derive constraints for detection rates from current upper bounds on the stochastic GW background produced by the same SMBH binary population that produces bursts with memory. The results and conclusions of this work are given in Section 5.

[3] While preparing this paper we became aware of a study by Pitkin (2012) that investigates burst localization using PTAs in detail.

2. SOURCES, SIGNATURES, AND RATES

GW bursts are expected from a wide variety of sources but we focus on BWMs from SMBH binaries because they provide the greatest opportunity for detection using pulsars. SMBH binaries will produce an oscillatory waveform in the dimensionless strain h during the inspiral phase that grows in amplitude until the objects merge in the plunge and ringdown stages. The memory effect comprises a DC offset in h that also grows on a time scale $2\pi R_s/c \sim M_9$ days to an asymptotic value $h_b \sim (\Delta M/M)R_s/D \sim 5 \times 10^{-15} M_9/D_{\rm Gpc}$. Here R_s is the Schwarzschild radius for the total mass $M = M_9 10^9\, M_\odot$ and $D_{\rm Gpc}$ is the distance in Gpc. This result follows from early estimates by Braginskii & Thorne (1987) and a rigorous treatment by Favata (2009), who showed that the mass fraction contributing to the memory effect $\epsilon = \Delta M/M \sim 0.07$; this quantity is dependent on the spins of the merging black holes (e.g., Pollney & Reisswig 2011). While similar amplitudes from tidal disruption events in globular clusters and the Galactic center will affect pulsars that are within $\sim$1 pc of these objects, event rates are far too small, e.g., $\sim 5 \times 10^{-5}$ yr^{-1} for the Galactic center (Brockamp et al. 2011), to allow for a plausible detection. In the following we write the burst amplitude as $h_b = C_h \mu/D_c$ where $C_h = \epsilon G/c^2$, μ is the reduced mass, and the comoving distance is $D_c = D_H \int_0^z dz\, [1/E(z)]$ with $D_H = cH_0^{-1}$ and we have used standard definitions as in Hogg (1999).

Seto (2009), van Haasteren & Levin (2010), and Pshirkov et al. (2010) use Favata's estimate for BWM amplitudes from black-hole mergers, which incorporates both the linear and nonlinear (Christopodeleu) contributions. While memory seems to be generic to bursts, its detection would be a strong confirmation of gravitational waves and nonlinearity in general relativity.

The waveform in h is a jump in the Doppler shift of a pulsar's pulse rate comprising two terms, one during the burst's arrival in the solar system, the other from arrival at the pulsar. The jump is effectively instantaneous because pulsar arrival times are measured at intervals much longer than the rise time of the burst. The arrival time perturbation is

$$\Delta t(t) = h_b B(\theta, \phi)\, [(t - t_0)\Theta(t - t_0) - (t - t_1)\Theta(t - t_1)]\,, \quad (1)$$

where h_b is the burst amplitude, $\Theta(t)$ is the Heaviside function, $t_1 = t_0 + D(1 - \cos\theta)/c$ and $\cos\theta = \hat{n} \cdot \hat{n}_g$ using unit vectors toward the pulsar ($\hat{n}$) and burst source ($\hat{n}_g$). The quantity $B(\theta, \phi) = (1/2)\cos 2\phi(1 - \cos\theta)$ describes the angular and GW polarization dependence of the time-of-arrival (TOA) perturbation, where we have adopted the notation of van Haasteren & Levin (2010); ϕ is the projected azimuthal angle of the pulsar's direction and the fiducial polarization direction of the GW in the plane perpendicular to $\hat{n}_g$. For a given burst, the effect in timing data from the pulsar term is never earlier than that in the Earth term.

Detection of a BWM requires matched filtering using a family of functions parameterized by the event time and the burst

amplitude. Implementation in the analysis of an individual time series by searching for a discontinuity in slope can reveal an event in either the pulsar term or in the Earth term of the perturbation, as discussed in Section 3. The sensitivity of the Earth-term analysis can be improved by a factor $\sim\sqrt{N_p}$ by coherently combining the time series of N_p pulsars. Following van Haasteren & Levin (2010), the sum of time series over N_p pulsars is

$$E_b(t) = \sum_{j=1}^{N_p} w_j \Delta t_j(t), \qquad w_j \propto B_j/\sigma_j^2 \equiv B(\theta_j, \phi_j)/\sigma_j^2, \tag{2}$$

where $\Delta t_j(t)$ is the timing residual versus epoch t for the jth pulsar. This notation implies that all pulsars are sampled at the same epoch; in actual sampled data, the residuals would be summed by using appropriate binning in time or by interpolation. The weights are based on the assumption that only white noise with variance σ_j^2 adds to the BWM and de-emphasize pulsars for which $|B(\theta, \phi)|$ is small. The resulting S/N is larger by a factor $\sqrt{N_p}$ over that in a single time series,

$$\begin{aligned} \mathrm{S/N}(E_b) &= h_b(t-t_b)\Theta(t-t_b)\left(\sum_j \frac{B_j^2}{\sigma_j^2}\right)^{1/2} \\ &= \sqrt{N_p} h_b \sigma^{-1}(t-t_b)\Theta(t-t_0)\langle B^2(\theta,\phi)\rangle_\Omega^{1/2}, \end{aligned} \tag{3}$$

where the second equality applies if all noise variances are the same and we use an average over an angular distribution of pulsars. For an isotropic distribution $\langle B^2(\theta, \phi)\rangle_\Omega = 1/6$.

2.1. Comparison of Earth and Pulsar Terms

To demonstrate the real advantage of focusing on the pulsar terms, we calculate the expected number of events that will occur in either the Earth or the pulsar terms in an analysis of N_p pulsars. The mean number of bursts in a single time series from either term (not both) is

$$N_b = T_{\rm eff}\eta(>h_{\rm min}) = T_{\rm eff}\int_{h_{\rm min}}^{\infty} dh\,\frac{d\eta}{dh}, \tag{4}$$

where $h_{\rm min}$ is the minimum detectable burst amplitude in a single data set, $T_{\rm eff}$ is the total effective observing time, and $d\eta/dh$ is the event rate per unit dh for strain amplitudes between h and $h+dh$. We show in Section 3 that a changepoint analysis on a single time series of length T has a roughly constant detection sensitivity for the central 70% of the time span, corresponding to $T_{\rm eff} \approx 0.7T$. Analysis of the correlated perturbation in the Earth terms for N_p pulsars yields a minimum detectable amplitude $h_{\rm min}/\sqrt{N_p}$. For the set of pulsar terms in N_p objects, the threshold amplitude is $h_{\rm min}$ but the aggregate observing time is $N_pT_{\rm eff}$. Assuming that $d\eta/dh \propto h^{-a}$, one can calculate the expected number of events in the Earth term, denoted $N_b^{(\rm E)}$, and in the pulsar terms, denoted $N_b^{(\rm P)}$:

$$N_b^{(\rm P)} = N_p\eta(>h_{\rm min})T_{\rm eff}, \qquad N_b^{(\rm E)} = N_p^{(a-3)/2}N_b^{(\rm P)}. \tag{5}$$

Their ratio, $r_{\rm PE} = N_b^{(\rm P)}/N_b^{(\rm E)} = N_p^{(3-a)/2}$, exceeds unity as long as the power-law index satisfies $a < 3$, meaning that more bursts will be detected in the pulsar terms than in the Earth terms.

The power-law index is determined by the spatial distribution of merging systems and by the distribution of their reduced masses. A set of standard candles corresponding to a fixed reduced mass with an unbounded distributed in Euclidean space has $d\eta/dh \propto h^{-4}$ or $a = 4$. This yields a burst ratio $r_{\rm PE} = N_p^{-1/2}$, implying for $N_p \gg 1$ that many more bursts will be seen in the Earth terms than in the pulsar terms. We suggest, however, that the power-law index may be small enough so that—if any bursts are seen—more will be seen in the pulsar terms than in the Earth terms. For a PTA with $N_p = 20$ pulsars, $r_{\rm PE}$ could represent a factor of two to three for plausible values of the index.

2.2. Preliminary Constraints on Rates and Amplitudes

Approximate bounds on the rate of BWMs can be made based on the observation that most of the timing residuals from MSPs analyzed in current pulsar timing arrays are consistent with white noise.[4] The total rms residual for a BWM and additive noise (with an rms amplitude σ_n) can be calculated after removing a second-order polynomial using Equations (17), (28), and (29) from Pshirkov et al. (2010),

$$\sigma_{\mathcal{R}} = \left[\sigma_n^2 + (h_bT)^2/3072\right]^{1/2}. \tag{6}$$

If we assume that no BWM has increased the residual variance, $\sigma_{\mathcal{R}}^2$, by a factor of $1+\epsilon$ in any of the time series, with $\epsilon = 0.1\epsilon_{0.1}$ the limit on the burst amplitude becomes

$$h_b \leqslant \sqrt{3072\epsilon}\frac{\sigma_n}{T} = 10^{-14.0}\frac{\epsilon_{0.1}\sigma_{100}}{T_5} \tag{7}$$

for $T = 5\,{\rm yr}\,T_5$ and $\sigma_n = 100\sigma_{100}$ ns. The fiducial value of ϵ is of the order of the estimation error on the variance when the residuals comprise only white noise, $\sqrt{2/N_t} \approx 0.06$ for $N_t = 512$ samples. A recent report on five pulsars in the European PTA sample (van Haasteren et al. 2011) timed over 5–10 years yields a median value $\sigma_n \approx 400$ ns. If only the Earth term is considered, this would imply $h_b < 10^{-13.7}$ and an upper bound on the rate of bursts larger than this amplitude $\eta(>h_{\rm min} = 10^{-13.7}) = 1/T_{\rm eff} \approx 0.3\ {\rm yr}^{-1}$. If we include the pulsar terms in the analysis, we can also constrain $\eta(>h_{\rm min}) = 1/(N_p+1)T_{\rm eff} \approx 0.05\ {\rm yr}^{-1}$ for bursts with amplitudes larger than $h_{\rm min} = 10^{-13.4}$. If we reference this rate to a lower, fiducial amplitude $h_0 = 10^{-15}$ for later comparison using $\eta_0 \equiv \eta(>h_0) = (h_{\rm min}/h_0)^{a-1}\eta(>h_{\rm min})$, we obtain $\eta_0 \lesssim 1.3\ {\rm yr}^{-1}$ for $a = 2$ and $\eta_0 \lesssim 60\ {\rm yr}^{-1}$ for $a = 3$. Similar constraints come from the Parkes Pulsar Timing Array (Yardley et al. 2011) and from the NANOGrav collaboration (Demorest et al. 2012).

3. EVENT DETECTIONS AND INFERENCES

Detecting a change in slope of the apparent pulse frequency is obviously best done in the time domain through a "changepoint" analysis (e.g., Ó Ruanaidh & Fitzgerald 1996). For low event rates we expect at most one event in the time series for any given pulsar (from either the Earth but more likely in the pulsar term). As pointed out by Pshirkov et al. (2010), a burst with signature $(t-t_b)\Theta(t-t_b)$ occurring in the interval $[0, T]$ will

[4] Consistency with white noise is in part a selection effect related to exclusion of two MSPs from the sample because they show red-noise contributions; as noted before in the text, one of these (B1821−24) has also shown a small discontinuity in spin rate that has been interpreted as a rotational glitch.

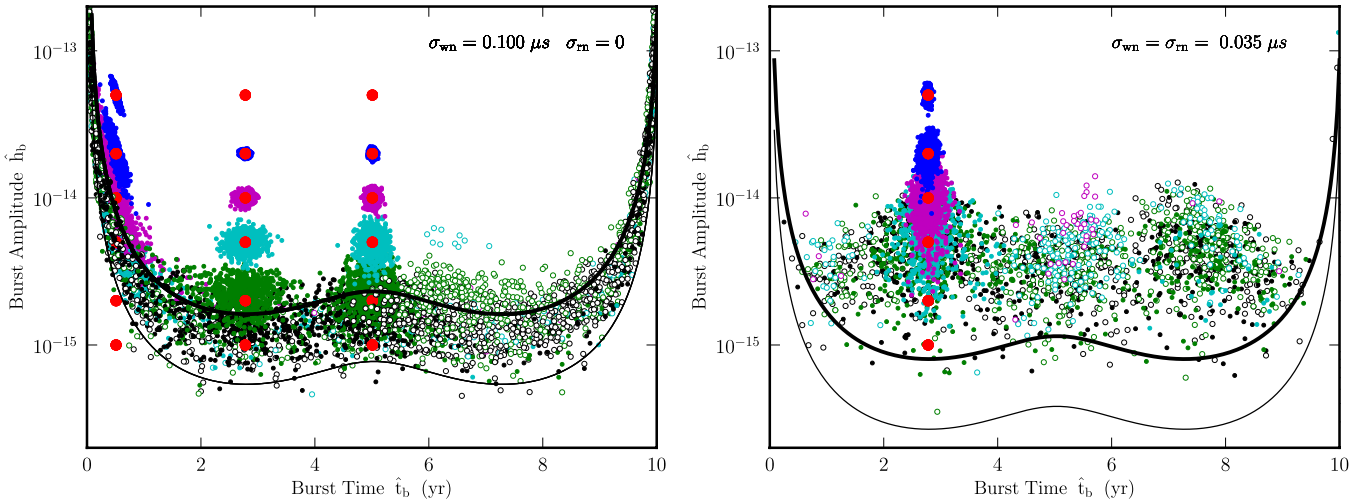

Figure 1. Scatter plot of estimates for the dimensionless strain jump amplitude h_b and epoch t_b obtained from least-squares fits to simulated data consisting of a ramp function and additive noise. Results were obtained using 512 arrival times in 1000 realizations for each value of burst amplitude. The large (red) circles at 2.78 and 5 yr indicate the amplitudes and epochs of the input GW bursts. Input amplitudes were $h_b = 10^{-15}, 2\times10^{-15}, 5\times10^{-15}, 10^{-14}, 2\times10^{-14}$, and 5×10^{-14}. Small, filled (open) circles denote estimated amplitude, $\hat{h}_b$, values that are positive (negative). The light and heavy wavy lines, respectively, represent 1σ and 3σ levels that apply to the case where additive noise only comprises white noise. For negligible burst amplitudes, most of the points would fall between these lines. (Left) Results for 100 ns of white noise only and for burst epochs of $(T/2)(1-1/\sqrt{5}) = 2.78$ yr, where the rms error on the estimated amplitude $\hat{h}_b$ is minimum, and $T/2$. (Right) Results for total rms noise of 50 ns that is equally split (quadratically) between white noise and red noise having an f^{-5} spectrum that represents intrinsic spin noise. (A color version of this figure is available in the online journal.)

have residuals from a second-order polynomial fit consisting of two piecewise parabolic components with the same constant and quadratic terms before and after the burst. The changepoint analysis involves stepping through all possible burst times t_b in the interval $[0^+, T^-]$ and fitting for h_b using the function

$$\Delta t(t) = p_0 + p_1 t + p_2 t^2 + h_b(t - t_b)\Theta(t - t_b). \quad (8)$$

The standard error in the least-squares fit for h_b has a minimum at burst epochs $(T/2)(1\pm1/\sqrt{5})$ (van Haasteren & Levin 2010),

$$\sigma_{h_b} \approx \left(\frac{1500}{N_t}\right)^{1/2} \frac{\sigma_n}{T} \approx 10^{-15.27}\sigma_{100}\left(\frac{512}{N_t}\right)^{1/2}\left(\frac{10\,\mathrm{yr}}{T}\right), \quad (9)$$

for $N_t \gg 1$ when the only errors are white noise.

This is comparable to the ~150 ns amplitude for a jump $h_b = 10^{-15}$ occurring in the inner 70% of the data span. At a significance $m\sigma$ the minimum detectable burst amplitude for a pulsar with angles θ, ϕ is $h_b B(\theta,\phi) \geqslant h_{\min} = m\sigma_{h_b}$. These results indicate that for $T = 10$ yr and rms white noise $\sigma_t = 100$ ns, a burst with $h_b B(\theta,\phi) \gtrsim 5\times10^{-15}$ would be detected at the 10σ level ($m = 10$) if the burst epoch is within the inner 70% of the data interval, i.e., $0.15T \leqslant t_b \leqslant 0.85T$. Thus the effective exposure time of a pulsar data set of length T is approximately $0.7T$.

In Figure 1 we show results from fitting simulated arrival-time data that include a BWM with a specified amplitude and epoch. The BWM signature was combined with white zero-mean Gaussian noise that represents TOA measurement errors and in some cases we also included red noise that represents contributions from spin fluctuations in the pulsar. We have used two burst epochs, 2.78 yr and 5 yr, in order to illustrate the variation in estimation errors in the fit parameters. We made a least-squares fit of Equation (8) for each possible value of the burst epoch t_b in the interval $[0, T]$, yielding an estimated burst amplitude $\hat{h}_b$ and epoch $\hat{t}_b$. The left-hand panel of Figure 1 shows the results for cases where the simulated data consist of the burst and white noise with 100 ns rms. The results verify the estimated detectability based on Equation (9). The right-hand panel includes red noise and is discussed in the next section.

3.1. False Positives from Red Noise

Red noise is also likely to add to white noise in TOA measurements. Canonical pulsars and magnetars with magnetic fields $\gtrsim 10^{11.5}$ G show red timing noise caused by processes in either the neutron star or magnetosphere or both. Plasma dispersion and scattering in the interstellar medium (ISM) will also contribute red noise. Since ISM contributions are highly chromatic, they can potentially be removed using multifrequency measurements, but simulations indicate that removal will not be complete (R. M. Shannon & J. M. Cordes, in preparation). More significantly, chromatic spin noise cannot easily be distinguished from GW signals, particularly the stochastic background from the ensemble of SMBH binaries, which is projected to have a power spectrum in timing residuals similar to that of timing noise. Here we describe how red noise will also increase the detection threshold for BWMs.

Recent work by Shannon & Cordes (2010) gives a scaling law for the rms timing residuals (after a second-order fit) from red spin noise that applies to both canonical pulsars and MSPs,

$$\sigma_r(T) \approx 138\,\mathrm{ns}\left(\frac{T}{10\,\mathrm{yr}}\right)^{2\pm0.2}\left(\frac{P}{5\,\mathrm{ms}}\right)^{1.4\pm0.1} \times \left(\frac{\dot{P}}{4\times10^{-15}}\right)^{1.1\pm0.1}. \quad (10)$$

We emphasize that the well known spin glitches are a different phenomenon and are not included in this scaling law. The scaling $\sigma_r \propto T^2$ is consistent with an f^{-5} power spectrum. While defining the overall trend, individual objects show large scatter about this relationship. In canonical pulsars, stochastic spin fluctuations appear to comprise step functions in the spin

rate or its derivative with a variety of event rates. In some objects, individual events are resolved while in others they are not (Cordes & Downs 1985; Lyne et al. 2010). Individual realizations of red noise show statistical changes in the slope of timing residuals that provide a noise floor for detecting BWMs.

We quantify changes in phase slope using the structure function for spin frequency $D_\nu(\tau) = \langle[\delta\nu(t+\tau) - \delta\nu(t)]^2\rangle$. The structure function can be related to the power spectrum of the spin fluctuations ($\propto f^{-5}$) and to the resulting rms residual, $\sigma_r \propto T^2$. We integrate the spectrum between a lower frequency limit ϵ/T, where $\epsilon \approx 1$ takes into account the high-pass filtering from a parabolic fit, and an upper limit $\kappa/\Delta t$, where Δt is a typical sample interval and $\kappa \approx 1/2$. The rms amplitude of apparent frequency jumps for $\tau \ll T$, following definitions in Cordes & Downs (1985, Equations (23)–(26) and Section VIb), can be shown to be

$$h_{b,\rm rms} = \frac{\sqrt{D_\nu(\tau)}}{\nu} = 8\pi^2\epsilon^2\left[\frac{\tau\sigma_r(T)}{T^2}\right]\sqrt{\ln\frac{\kappa T}{\epsilon\Delta t}}$$
$$\approx 10^{-14.2}\epsilon^2\sigma_{r,100}(T = 10\,{\rm yr})\tau_{\rm yr}. \quad (11)$$

We have evaluated $h_{b,\rm rms}$ for a nominal value of the rms red noise, $\sigma_r = 100$ ns, over a 10 yr time span and for a time lag of 1 yr. The latter choice corresponds to a changepoint analysis made by fitting the residuals for 1/2 year before and after a specific epoch. Longer fitting spans correspond to larger effective time lags with larger values of $h_{b,\rm rms}$. However, Equation (11) is based on the assumption that $\tau \ll T$ and is intended to give only a rough estimate of the amplitudes of pseudo jumps in spin frequency. Values for ϵ are given in Table 1 of Blandford et al. (1984) and are $\sim$1 for an f^{-5} spectrum.

The scaling law implies that 100 ns residuals, if produced by a red-noise process, would show statistical changes $h \approx 10^{-14}$ on time scales of a year. Red-noise levels in MSPs appear to be smaller than 100 ns in most cases (e.g., Demorest et al. 2012) so the pseudo jumps will accordingly be smaller.

Figure 1 (right panel) shows simulations where equal amounts of white and red noise have been added to the burst perturbation, for a total rms noise of 50 ns. The red noise has a strong deleterious effect on burst detection compared to the case in the left-hand panel which has only white noise and at a level that is twice as large as the total in the right-hand panel.

Diagnosing particular candidate changepoints can exploit the fact that more than one pseudo changepoint is likely to occur in a realization of a red-noise process. If a real BWM occurs in a data set that is combined only with white noise, a test before and after the burst epoch should be consistent with white noise. Partitioning of the data set into halves, quarters, etc., will show pseudo changepoints in all data subspans if there is only red noise in the data and no real changepoint.

3.2. Inferences about Burst Rates from Possible Detection Scenarios

Given that burst rates from SMBH binary mergers are probably small ($\lesssim$0.1 yr^{-1}), plausible scenarios in a timing program of N_p pulsars include the three cases where (1) no BWMs will be detected at all; (2) a single BWM will be detected in one of the pulsar terms and none in the Earth terms; and (3) a single burst will be detected in a coherent analysis of the Earth terms but not in any of the N_p pulsar terms. The Poisson probabilities of seeing no events in either the Earth or pulsar terms are

$$P_0({\rm E}) = e^{-N_b^{({\rm E})}} = e^{-\eta(>h_{\rm min})/\eta_{E,0}}, \quad (12)$$

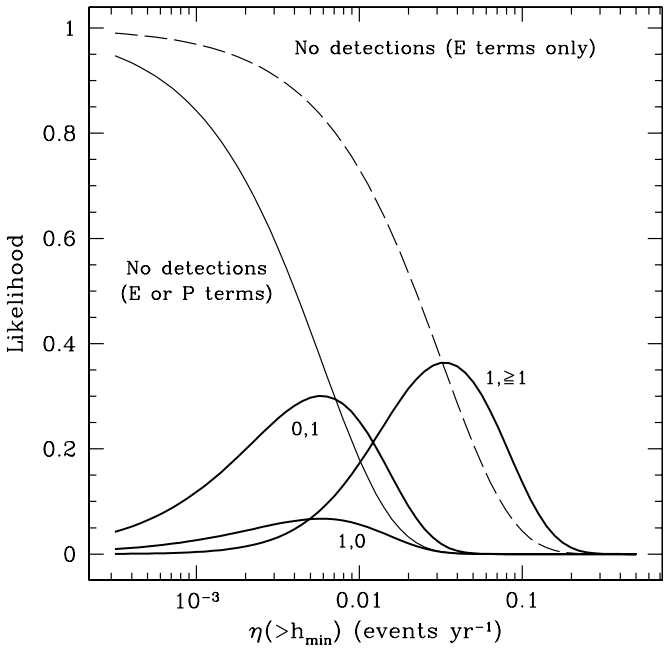

Figure 2. Likelihood functions for detection of BWMs as a function of the burst rate for events that are above threshold. The "No detections" curves give the likelihoods for the cases where no events are seen in the Earth terms (dashed line) or in the combination of Earth and pulsar terms (solid line). The other curves represent the cases where zero and one events are seen in the Earth and pulsar terms (0,1), or one and zero (1, 0), respectively, or one event in the Earth terms and at least one event in the pulsar terms (1, $\geqslant$ 1). The plots shown are for a PTA with $N_p = 20$ pulsars. Note that the curves are for an index $a = 2$ in the distribution $d\eta/dh \propto h^{-a}$. Other cases are discussed in the text.

$$P_0({\rm P}) = e^{-N_b^{({\rm P})}} = e^{-\eta(>h_{\rm min})/\eta_{P,0}}, \quad (13)$$

where the e-folding rates are defined as $\eta_{\rm P,0} = 1/N_p T_{\rm eff}$ and $\eta_{\rm E,0} = r_{\rm PE}\eta_{\rm P,0}$ and we have used the ratio $r_{\rm PE}$ defined in Section 2.1 just below Equation (5). Even though the Earth term constrains events as weak as $h_{\rm min}/\sqrt{N_p}$, we have extrapolated this limit to the larger strain, $h_{\rm min}$, by using the ratio $r_{\rm PE}$ that depends implicitly on a. For $a < 3$ the pulsar terms are more constraining on the rate. The probabilities of seeing single events are $P_1({\rm E}) = N_b^{({\rm E})}P_0({\rm E})$ and $P_1({\rm P}) = N_b^{({\rm E})}P_0({\rm P})$. From these we calculate likelihood functions for the fiducial rate $\eta_0 = \eta(>h_0)$ that is referenced to an amplitude h_0. For case 1 the likelihood function is $L_{00} = P_0({\rm E})P_0({\rm P})$ while for case 2 we have $L_{01} = P_0({\rm E})P_1({\rm P})$. A less likely case for a shallow distribution (e.g., $a \leqslant 2$) is case 3, for which $L_{10} = P_0({\rm P})P_1({\rm E})$. A more detailed approach would treat each time series individually to account for differences in data quality, but the principle is the same.

Figure 2 shows likelihood functions assuming a shallow amplitude distribution $a = 2$.

We have assumed data sets for $N_p = 20$ pulsars of length $T = 10$ yr and we have taken into account that only 70% of the data span provides adequate sensitivity. The results are based on an assumed detection threshold for the Earth-term analysis that is smaller by a factor $1/\sqrt{N_p}$. We also show (dashed curve) the likelihood function for the case where only the Earth terms are considered and no events are seen; the likelihood function is then just $P_0({\rm E})$. Comparison with the combined likelihood function for no detections in either the pulsar terms or the Earth terms (solid line) shows that an upper bound on the event rate for the combined case is indeed smaller by $1/\sqrt{N_p} \approx 0.22$, in

accordance with the ratio $r_{\rm PE}$ defined in Section 2.1 for $a = 2$. Use of a larger number of pulsars shifts the curves to the left. A shallower amplitude distribution with $a < 2$ raises the $N_b^{(\rm P)}$ curve higher relative to the $N_b^{(\rm E)}$ curve at fixed $\eta(>h_{\rm min})$. For $a = 3$, the $N_b^{(\rm P)}$ and $N_b^{(\rm E)}$ curves are identical, as expected. For standard candles in Euclidean space ($a = 4$), the detection of a single event in the Earth terms becomes much more likely than in one of the pulsar terms.

The results shown in Figure 2 are schematic but indicative of what can be concluded from existing data. As shown in the first part of this section, 10 year PTA data sets with 100 ns of white noise allow detections above $h_{\rm lim} \approx 5 \times 10^{-15}$. Some current data sets have rms white-noise residuals smaller than 100 ns but most are larger (van Haasteren et al. 2011; Yardley et al. 2011; Demorest et al. 2012). In addition, not all data sets are 10 year long. With heterogeneous data sets and in advance of a specific analysis on existing PTA data, the results in Figure 2 cannot be taken literally. However, they do indicate that event rates are likely to be in the range of 0.01 to 0.1 events yr^{-1} for $h_{\rm lim} = 5 \times 10^{-15}$.

4. CONSTRAINTS ON THE BURST DETECTION RATE FROM THE GW STOCHASTIC BACKGROUND

Another way of assessing the GW burst rate is to calculate constraints based on current upper bounds on the stochastic GW background that have been made with PTAs. We again find that a wide range of burst rates is allowed.

Following others (Phinney 2001; Jaffe & Backer 2003), we calculate the event rate $d\eta/dh$ by integrating over the probability density function (PDF) for the SMBH masses, $f_m(m; z)$, which may be redshift dependent as indicated, and the redshift-dependent merger rate per unit comoving volume, $R(z)$. Assuming statistical independence of the merging masses, the differential rate is

$$\frac{d\eta}{dh} = \frac{4\pi C_h^3}{h^4} \int\int dm_1 dm_2\, f_m(m_1; \hat{z}) f_m(m_2; \hat{z}) \frac{\mu^3 R(\hat{z})}{(1+\hat{z})}, \tag{14}$$

where $\hat{z}$ is the solution of $\hat{z} = \hat{z}(\hat{D}_c)$ and the comoving distance is $\hat{D}_c = C_h \mu/h$ (where C_h is defined in Section 2). Equation (14) shows an explicit scaling $\propto h^{-4}$ but there is additional dependence in $\hat{z}$ that can make the net scaling shallower. Cosmic evolution skews the mass PDF to larger masses at low redshift that more than compensates the smaller $R(z)$ at low z in determining the observed merger rate. Enoki et al. (2004) show that the overall merger rate is larger at high redshifts, that the SMBH mass evolves to higher masses, and the largest burst amplitudes are dominated by low-z, high-mass mergers. Similar results are given in Sesana et al. (2008). Figure 6 of Enoki et al. (2004) shows that the burst rate for large amplitudes has a slope corresponding to $a \approx 2$. Unfortunately, the authors assumed that the burst amplitude scaled as the total mass of the system as opposed to the reduced mass. Hence, the result shown in Enoki et al.'s Figure 6 is not applicable to the bursts we are considering in this work.

Using a Monte Carlo analysis, we verified that one can achieve a shallow scaling law by drawing masses from a power-law distribution that scales as the $-3/2$ power or greater. This is not inconsistent with previously estimated mass functions (i.e. Caramete & Biermann 2010). We used a merger rate $R(z)$ related to Enoki et al.'s $\nu(z) = 4\pi c D_c^2 R(z)/H_0(1+z)E(z)$ and find that $d\eta/dh \propto h^{-2}$ in ranges of dimensionless strain that depend on the upper mass cutoff. For $M_{\rm max} = 10^{10}\, M_\odot$, for example, the inverse quadratic scaling applies for $10^{-18} \lesssim h \lesssim 10^{-15}$ and the ratio of events is $r_{\rm PE} \approx 2.0$ for 20 pulsars assuming a minimum detectable strain of 10^{-15} for a single pulsar.

We constrain $\eta(< h_{\rm min})$ by using current limits on the *stochastic* GW background produced by inspiraling SMBHs prior to merging. We factor the merger rate as $R(z) = R_0[R(z)/R_0]$ where R_0 is the rate at $z = 0$, and then write

$$\begin{aligned}\eta(>h_{\rm min}) &= 4\pi D_H^3 R_0 \int\int dm_1 dm_2\, f_{m;\hat{z}}(m_1) f_m(m_2; \hat{z}) J_\eta(s) \\ &\equiv 4\pi D_H^3 R_0 \left\langle J_\eta(s) \right\rangle_m , \end{aligned} \tag{15}$$

where $s = C_h \mu/D_H h_{\rm min}$ and we define the dimensionless integral

$$J_\eta(s) = \int_0^s dx\, x^2 \left[\frac{R(\hat{z})/R_0}{1+\hat{z}}\right]. \tag{16}$$

The average of $J_\eta(s)$ over the double mass integral in Equation (15) is denoted with angular brackets as $\left\langle J_\eta(h_{\rm min})\right\rangle_m$ and having an argument $h_{\rm min}$. For standard candles corresponding to the case where f_m is a delta function combined with a scaling of event rate with redshift, $R(z) \propto 1+z$, would yield $\eta(>h_{\rm min}) \propto h_{\rm min}^{-3}$. In general, however, the scaling of $\eta(>h_{\rm min})$ is shallower in $h_{\rm min}$ because the mass PDF evolves with redshift toward larger mean masses, as borne out by previous work cited above.

Using fiducial numbers

$$\begin{aligned}\eta(>h_{\rm min}) &= C_\eta \left[\frac{R_0}{R_0({\rm JB})}\right] \langle J_\eta(h_{\rm min})\rangle_m \\ C_\eta &= 4\pi D_H^2 R_0({\rm JB}) = 0.031 \text{ events yr}^{-1}, \end{aligned} \tag{17}$$

where $R_0({\rm JB}) = 3.14 \times 10^4$ events Gyr^{-1} Gpc^{-3} is the rate assumed by Jaffe & Backer (2003).

For the stochastic GW background, an approach similar to that for the burst rate yields the rms dimensionless strain, $h_c(f)$, in a band centered on f and we adopt the power-law form $h_c(f) = Af^{-2/3}$ with the GW frequency in cycles yr^{-1}:

$$A^2 = C_{\rm sbg} \left(\frac{\mathcal{M}_c}{\mathcal{M}_{c,{\rm nom}}}\right)^{5/3} \left[\frac{R_0}{R_0({\rm JB})}\right] J_{h_c} \tag{18}$$

$$\begin{aligned} C_{\rm sbg} &= \frac{4\pi D_H c^{1/3} (G/c^2)^{5/3}}{3\pi^{4/3}} M_{c0} R_0({\rm JB}) \\ &\quad \times (1 \text{ cy yr}^{-1})^{-4/3} = 10^{-32.0} \end{aligned} \tag{19}$$

$$J_{h_c} = \int dz\, \frac{R(z)}{R_0} \frac{\left\langle \mathcal{M}_c^{5/3}\right\rangle_m}{\mathcal{M}_{c,{\rm nom}}^{5/3}} \frac{1}{(1+z)^{4/3} E(z)}, \tag{20}$$

where the characteristic chirp mass M_c calculated from the mass distribution is $\mathcal{M}_c = \langle M_c^{5/3}\rangle_m^{3/5}$ and a nominal value $\mathcal{M}_{c,{\rm nom}} = 2.3 \times 10^7\, M_\odot$ has been used to estimate the dimensionless coefficient[5] $C_{\rm sbg}$ for GW frequencies f expressed in cycles yr^{-1}. For other values of $\mathcal{M}_c$, Equation (18) includes

[5] Our value differs from that implied in Equation (32) of Jaffe & Backer (2003) using the same nominal chirp mass, $(1.27 \times 10^{-15})^2$. It appears that their value is for a larger chirp mass of $5 \times 10^8\, M_\odot$.

the scaling relative to the nominal value. As with the burst rate $\eta(>h_{\rm min})$, the stochastic background depends on the redshift dependence of the merger rate and mass distributions. Sesana et al. (2008) show that $h_c^2(f)$ is dominated by a relatively small number of mergers taking place at low redshifts with the largest chirp masses.

Recent work has placed limits on A using various analyses of pulsar timing data. For a limit $A_{\rm lim}$ we derive an upper bound on the merger rate R_0 and then an upper bound on the observed burst rate $\eta(>h_{\rm min})$,

$$\eta(>h_{\rm min}) < A_{\rm lim}^2 \left(\frac{C_\eta}{C_{\rm sbg}}\right)\left(\frac{\mathcal{M}_{c,\rm nom}}{\mathcal{M}_c}\right)^{5/3} \frac{\langle J_\eta(h_{\rm min})\rangle_m}{J_{h_c}}. \quad (21)$$

For an upper bound on the spectral coefficient, $A_{\rm lim} = 10^{-14}A_{\rm lim,-14}$, and nominal values for the chirp mass and other quantities, the observed rate limit is

$$\eta(>h_{\rm min}) < 0.32 \text{ events yr}^{-1} A_{\rm lim,-14}^2 \times \left(\frac{\mathcal{M}_{c,\rm nom}}{\mathcal{M}_c}\right)^{5/3} \frac{\langle J_\eta(h_{\rm min})\rangle_m/10^{-3}}{J_{h_c}}. \quad (22)$$

Limits on the stochastic background have decreased steadily from $A_{\rm lim} = 1.1\times10^{-14}$ (Jenet et al. 2006) to $A_{\rm lim} = 6\times10^{-15}$ (van Haasteren et al. 2011) and are expected to decrease to 10^{-15} or less using results from ongoing timing programs. These limits imply that the burst rate could be quite large but the other factors in Equation (22) must be considered. Jaffe & Backer (2003) give a range $0.1 \lesssim J_{h_c} \lesssim 100$ for various redshift dependences of the merger rate and mean chirp mass. The burst-rate average $\langle J_\eta(h_{\rm min})\rangle_m$ can range from approximately unity to very small values that depend strongly on the mass distribution, merger rate versus redshift, and the detection limit, $h_{\rm min}$. Using Monte Carlo simulations for a mass distribution scaling as $m^{-3/2}$ (independent of redshift) with cutoffs at $10^5\,M_\odot$ and $10^{10}\,M_\odot$ we obtain $J_\eta(h_{\rm lim} = 10^{-15}) = 3\times10^{-4}$ and $J_{h_c} = 4.5$. These values imply an observed rate of only 0.02 events yr^{-1}. A lower threshold for bursts of $h_{\rm lim} = 10^{-16}$ yields a rate that is 20 times larger or 0.4 events yr^{-1}, which would imply that many events have occurred in existing PTA data although at levels too small to detect. Other mass distributions and mass cutoffs yield a wide range of observed rates. These results are broadly consistent with the schematic results presented in the previous section.

We conclude that the actual burst rate is essentially unconstrained by current PTA constraints on the stochastic background and that direct constraints on burst rates from pulsar timing data based on changepoint analyses will provide insight into the unknown quantities. A great deal of uncertainty exists about the rate of inspirals and burst rates based on surveys for binary SMBHs (e.g., Burke-Spolaor 2011). For now it is possible that the burst rate is large enough so that detections of bursts in the near future are possible.

5. DISCUSSION

We have shown that bursts with memory may occur at rates that make a detection plausible as pulsar timing programs accrue observing time on more MSPs.

Testing the reality of a candidate detection is problematic if an event is seen, for example, in a single time series out of an array of MSPs distributed widely in the Galactic disk. However, the distinctness of the signature—a ramp function in pulse phase—can be tested using longer data spans. Furthermore, in a program comprising a total pulsar-time product N_pT that detects one BWM, doubling the product may yield an additional detection unless the first detection is statistically fortuitous. Finally, globular clusters may provide a special opportunity to detect the same burst in multiple MSPs within the same globular cluster. There could be time offsets of less than 10 years between the appearance of a burst in the timing data for different MSPs. Typically, MSPs in globular clusters have been excluded in PTAs because of the effects of the stochastic gravitational potential in the cluster. However, the distinct, sharp discontinuity of the BWM signature may obviate the problems of using cluster MSPs for burst detection.

Merging SMBH binaries are the most plausible source of detectable BWMs as well as contributing in earlier stages to the stochastic GW background that is also sought with pulsar timing. If, as we have argued, BWMs are more likely to occur in the pulsar terms rather than the Earth terms of the overall timing perturbation, BWMs will appear as timing perturbations that are uncorrelated between objects. If their ramp signature is not recognized as such, the timing perturbation will contribute to the overall stochastic noise confusion that can mask the GW stochastic background.

In addition to BWMs, the changepoint analysis described in Section 3 may reveal events from other source classes. One of these consists of cosmic strings that produce GW bursts through cusps and kinks associated with string reconnection events. When a string crosses the line of sight to a pulsar, a direct (non-GW) event is detectable with a signature that is identical to the BWM signature, a ramp function in timing perturbation (Pshirkov & Tuntsov 2010).

Another perturbation that may also appear in MSP timing programs with large N_pT is from low-mass objects, such as primordial black holes, that pass within ~1000 AU of the Sun (Seto & Cooray 2007). The acceleration pulse imparted to the Sun will produce a rounded step-like function in apparent spin frequency of a pulsar that has a rise time of ~20 yr. Only in very long timing programs will this kind of event be separable from the spin parameters of the pulsar.

As a final comment, we note that electromagnetic counterpart events to BWMs will be seen nearly simultaneously in the Earth terms but will *precede* BWMs seen in a pulsar term by $(D/c)(1-\cos\theta)$ where θ is the pulsar–GW-source angle. Apart from fortuitous geometries that make this delay less than the data span length, counterpart events will be difficult to recognize unless they are very distinctive and last for hundreds to thousands of years.

We thank Tom Loredo for a useful discussion about extreme value statistics, M. Enoki for providing numerical versions of the results presented in Figure 6 of Enoki et al. (2004), D. Madison for comments on the manuscript, and an anonymous referee for a helpful review. We thank the NANOGrav collaboration for useful comments on this work. At Cornell University, this work was supported by the NSF through a subaward from grant AST 0968296 to West Virginia University. At University of Texas, Brownsville, this work was supported by NSF grants AST 0545837 and OISE 0968296.

REFERENCES

Blandford, R., Romani, R. W., & Narayan, R. 1984, J. Astrophys. Astron., 5, 369

Braginskii, V. B., & Thorne, K. S. 1987, Nature, 327, 123
Brockamp, M., Baumgardt, H., & Kroupa, P. 2011, MNRAS, 418, 1308
Burke-Spolaor, S. 2011, MNRAS, 410, 2113
Caramete, L. I., & Biermann, P. L. 2010, A&A, 521, A55
Cognard, I., & Backer, D. C. 2004, ApJ, 612, L125
Cordes, J. M., & Downs, G. S. 1985, ApJS, 59, 343
Demorest, P. B., Ferdman, R. D., Gonzalez, M. E., et al. 2012, arXiv:1201.6641
Enoki, M., Inoue, K. T., Nagashima, M., & Sugiyama, N. 2004, ApJ, 615, 19
Favata, M. 2009, ApJ, 696, L159
Finn, L. S., & Lommen, A. N. 2010, ApJ, 718, 1400
Hogg, D. W. 1999, arXiv:astro-ph/9905116
Jaffe, A. H., & Backer, D. C. 2003, ApJ, 583, 616
Jenet, F. A., Hobbs, G. B., van Straten, W., et al. 2006, ApJ, 653, 1571
Lyne, A., Hobbs, G., Kramer, M., Stairs, I., & Stappers, B. 2010, Science, 329, 408
Ó Ruanaidh, J. K., & Fitzgerald, W. J. 1996, Numerical Bayesian Methods Applied to Signal Processing (Berlin: Springer)
Phinney, E. S. 2001, arXiv:astro-ph/0108028
Pitkin, M. 2012, arXiv:1201.3573
Pitkin, M., Reid, S., Rowan, S., & Hough, J. 2011, Living Rev. Relativ., 14, 5
Pollney, D., & Reisswig, C. 2011, ApJ, 732, L13
Pshirkov, M. S., Baskaran, D., & Postnov, K. A. 2010, MNRAS, 402, 417
Pshirkov, M. S., & Tuntsov, A. V. 2010, Phys. Rev. D, 81, 083519
Sesana, A., Vecchio, A., & Colacino, C. N. 2008, MNRAS, 390, 192
Seto, N. 2009, MNRAS, 400, L38
Seto, N., & Cooray, A. 2007, ApJ, 659, L33
Shannon, R. M., & Cordes, J. M. 2010, ApJ, 725, 1607
van Haasteren, R., & Levin, Y. 2010, MNRAS, 401, 2372
van Haasteren, R., Levin, Y., Janssen, G. H., et al. 2011, MNRAS, 414, 3117
Yardley, D. R. B., Coles, W. A., Hobbs, G. B., et al. 2011, MNRAS, 414, 1777